Chemistry by Number Theory

Jan C.A. Boeyens and Peter Comba

Abstract Aspects of elementary number theory pertaining to the golden ratio and the golden spiral are shown to be related to and therefore of importance in the simulation of chemical phenomena. Readily derived concepts include atomic structure, electronegativity, bond order, the theory of covalent interaction and aspects of molecular chirality. The physical interpretation of the results implicates the 4D structure of space-time as a fundamental consideration. The implied classical nature of 3D molecular structure identifies molecular mechanics as an ideal method for structure optimization, and it is shown that the parameters may be related to number theory. All results point at a 4D wave structure of electrostatic charge.
Keywords: atomic structure, bond order, electronegativity, golden ratio, periodic function

1 Introduction

One of the most mysterious observations in Nature is the appearance of a single parameter that determines the macroscopic structure of a large variety of apparently unrelated objects, such as the distribution of florets in a composite seed head [1], the periodic table of the elements [2], the flight path of a predator bird in pursuit of its prey, the curvature of a kudu horn [1] and the surface features of a nanoparticle [3]. This ubiquitous parameter, known as the *golden ratio*, has also been called the *divine proportion* and for millenia has been used in architectural design, as a measure of human anatomical features, in works of art and in musical composition [1].

Corresponding author: Jan C.A. Boeyens
Centre for Advanced Scholarship, University of Pretoria, South Africa
e-mail: Jan Boeyens<jan.boeyens@up.ac.za>

Peter Comda
Anorganisch-Chemisches Institut, Universität Heidelberg
e-mail: Comba, Peter <Peter.Comba@aci.uni-heidelberg.de>

The periodic table of the elements is one of the first and most important concepts in chemistry, and we consider its relation to the golden ratio as compelling evidence that number theory could provide a significant basis of theoretical chemistry. In order to explore this contingency it is necessary to examine the relevant properties of the remarkable golden parameter in more detail.

2 The Golden Ratio

Mathematically, the golden ratio is formulated by the division of a unit line into two segments. An intermediate point on the line [ABC] divides the line in mean and extreme ratios AB/BC and BC/AB, BC>AB.

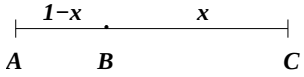

At the point where

$$\frac{AB}{BC} = \frac{BC}{AC}; \quad \frac{1-x}{x} = \frac{x}{1},$$

the section is described by the quadratic equation

$$x^2 = 1 - x \tag{1}$$

i.e.

$$\begin{aligned} 2x &= -1 \pm \sqrt{5} \\ x &= 0.61803\ldots \text{ or } \quad -1.61803\ldots \end{aligned}$$

This so-called golden section or golden ratio is defined by either of the irrational numbers

$$\tau = 0.61803\ldots \quad \text{or} \quad \Phi = 1.61803\cdots = \frac{1}{\tau}$$

This result follows on substituting $x = 1/x$ in (1). Multiplication by τ^n:

$$\tau^{n+2} = \tau^n - \tau^{n+1},$$

shows that any power of τ (or Φ) can be written as the difference between smaller powers. For example:

$$\begin{aligned} \tau^6 &= \tau^4 - \tau^5 \\ &= 2\tau^4 - \tau^3 \\ &= 2(\tau^2 - \tau^3) - (\tau - \tau^2) \\ &= 2(2\tau^2 - \tau) - (2\tau - 1) \\ &= 2(2 - 3\tau) - (2\tau - 1) \\ &= 5 - 8\tau \end{aligned}$$

Any power reduces to this form, in which the coefficients are successive terms in the Fibonacci series

$$0, 1, 1, 2, 3, 5, 8, 13, 21, \ldots$$

in which any term is the sum of the two preceeding terms, *i.e.*:

$$F_{n+1} = F_n + F_{n-1}\,, n > 0, F_1 = 1\,.$$

A general power of τ therefore becomes

$$\tau^n = F_{n-1} - F_n\tau\,.$$

It follows that

$$\begin{aligned}\lim_{n\to\infty} \frac{F_{n-1}}{F_n} &= \lim_{n\to\infty} \left(\frac{\tau^n}{F_n} + \tau\right) \\ &= \tau\,.\end{aligned}$$

The golden ratio is expressed as a trigonometric function in the form:

$$\tau = 2\cos\left(\frac{2\pi}{5}\right) \qquad \Phi = 2\cos\left(\frac{\pi}{5}\right).$$

It is therefore not surprising that the golden mean turns up in problems of five-fold symmetry. In particular, it is found that the diagonal of a unit pentagon,

$$d = \sqrt{1+1-2\cos(3\pi/5)} = \Phi$$

has the measure of the golden mean, as in Fig. 1. By noting that the quadrilateral

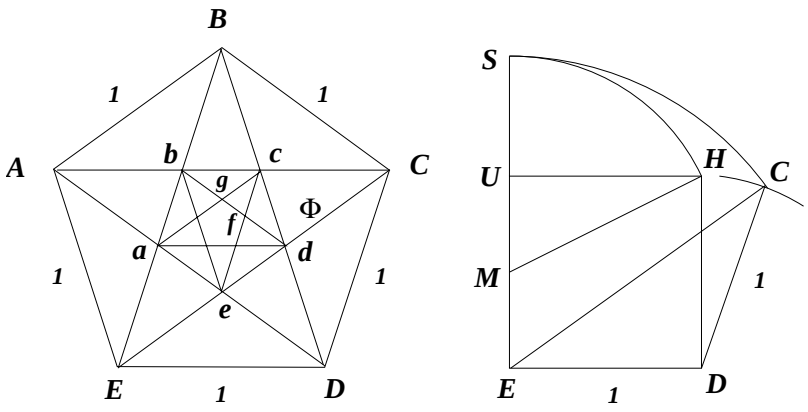

Fig. 1 *Diagram to demonstrate Euclid's construction of a regular pentagon and the golden section.*

ABCe is a paralellogram and that $\triangle ACe$ and $\triangle DEe$ are similar triangles, it follows

that

$$\frac{AD}{Ae} = \frac{Ae}{eD},$$

which means that the intersecting diagonals divide one another in golden ratio.

Euclid used this property to construct a regular pentagon, starting from a unit square. A circle, centred at the midpoint (M) of one side, intersects the extension of that side at S. By construction

$$MS = MH = \sqrt{5}MU = SU + \tfrac{1}{2} = \Phi - \tfrac{1}{2}.$$

Hence, $SU = \Phi - 1 = \tau$ and $AC = \Phi$, the diagonal of a unit pentagon. This process, repeated twice, yields the complete pentagon.

The distances BD, Bd, Bc, cd, cf, fg, are in geometrical progression, equal to

$$\Phi, 1, \Phi^{-1}(\tau), \Phi^{-2}(\tau^2), \tau^3, \tau^4, etc.$$

The construction of smaller or larger pentagrams around the central pentagon can be continued indefinitely to define an infinite geometrical series based on τ:

$$S = \{\Phi^n, n = -\infty, \infty\} \tag{2}$$

and the corresponding infinite structure consisting of self-similar pentagrams.

In the same way, addition of a line segment of length τ to a unit line yields the extended line [ABC], again divided in golden ratio by the intermediate point B, as before. This process, when continued indefinitely, generates a sequence of larger and larger copies of the original line in golden section. The same process unfolds in the opposite sense to create ever smaller copies. This property, called *self-similarity*, is vividly illustrated by the definition of τ as a continued fraction:

$$x = 1 + \frac{1}{1 + \frac{1}{1 + \frac{1}{1 + \frac{1}{1+\ldots}}}} = 1 + \frac{1}{x}; \quad x = 1 + \tau$$

Truncation of the algorithm at finite steps generates a series of rational fractions that converges to $1 + \tau = \Phi$. The convergents are the numbers

$$1, 1+1 = 2, 1 + \frac{1}{1+1} = \frac{3}{2}, 1 + \frac{1}{1 + \frac{1}{1+1}} = \frac{5}{3}, etc.$$

This sequence of fractions are given by

$$\left(\frac{m}{n}\right)_i = \frac{1}{1}, \frac{2}{1}, \frac{3}{2}, \frac{5}{3}, \frac{8}{5}, \frac{13}{8}, \ldots,$$

a series of Fibonacci fractions, as before.

Self-similarity is illustrated particularly well as the property of a Fibonacci *tree*, which contains infinituple copies of itself as shown in Fig. 2. Each black dot represents the start of a fresh tree.

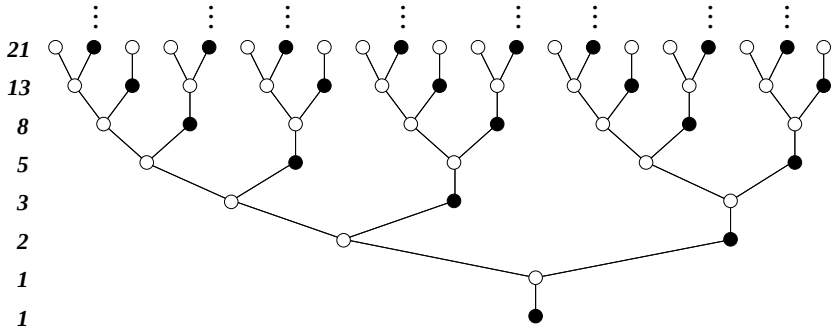

Fig. 2 *The Fibonacci tree that contains an infinite number of copies of itself.*

The self-similarity associated with the golden section is embodied geometrically in the spiral inscribed within a rectangle with sides in golden ratio. Removal of a square (gnomon) from such a golden rectangle leaves a smaller golden rectangle as residu. On continuing the process indefinitely rectangles of diminishing size are created, as shown in Fig. 3.

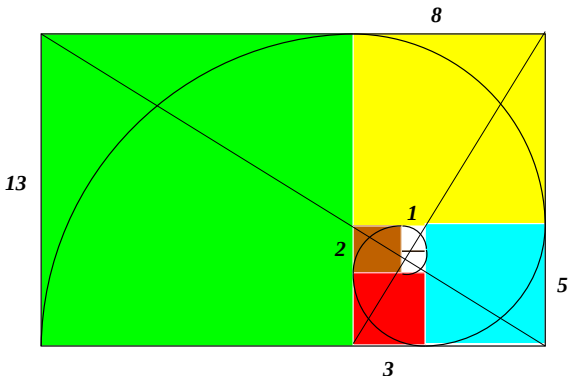

Fig. 3 *A Fibonacci spiral inscribed in a rectangle defined by a Fibonacci sequence. The increasing size of successive squares is defined by the Fibonacci labels* (n) *and the ratio of their side lengths approaches* τ *as* $n \to \infty$*. The inscribed spiral approximates a golden spiral and also an equiangular logarithmic spiral [4].*

To good approximation, the side lengths of successive gnomons decrease in line with the Fibonacci numbers, such that Fibonacci squares cover the composite golden rectangle, *e.g.*

$$1^2 + 1^2 + 2^2 + 3^2 + 5^2 + 8^2 + 13^2 = 13 \times (13 + 8) = 13 \times 21.$$

Likewise, the first n rectangles in a Fibonacci sequence cover the largest gnomon for n odd, *e.g.*

$$(1\times1)+(1\times1)+(1\times2)+(2\times3)+(3\times5)+(5\times8)+(8\times13)+(13\times21)=21^2$$

Circular segments inscribed between opposite vertices of the growing gnomons define a spiral which is approximated by the logarithmic spiral

$$r=ae^{\theta\cot\varphi},\ \varphi=72.9^\circ,\ \cot\varphi=\tau/2\,,$$

in which a and φ are constants and the angle θ defines the dilative rotation.

3 The Periodic Function

Èmile de Chancourtois, co-discoverer of elemental periodicity claimed [5] that

> ... the properties of the elements are the properties of numbers.

His claim was vindicated with the discovery of atomic number, but the theme remained undeveloped until it was conjectured by Peter Plichta [6] that the electron configuration of atoms is mapped by the distribution of prime numbers. Based on the

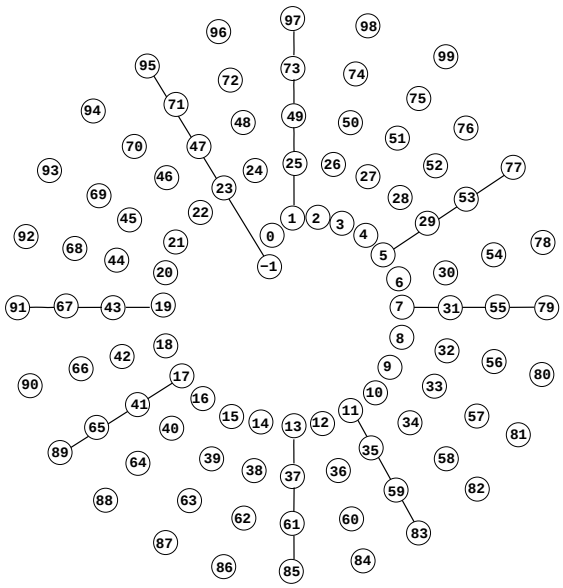

Fig. 4 *The natural numbers arranged on a spiral with a period of 24. All prime numbers* >3 *and of the form* $6n\pm1$ *occur on eight straight lines of the cross, which has been interpreted [6] to simulate the electronic structure of atoms.*

observation that all prime numbers > 3 are of the type $6n \pm 1$ he defined a prime-number cross that intersects a display of natural numbers on a set of concentric circles with a period of 24. In Fig. 4 the construct is shown, rearranged as a number

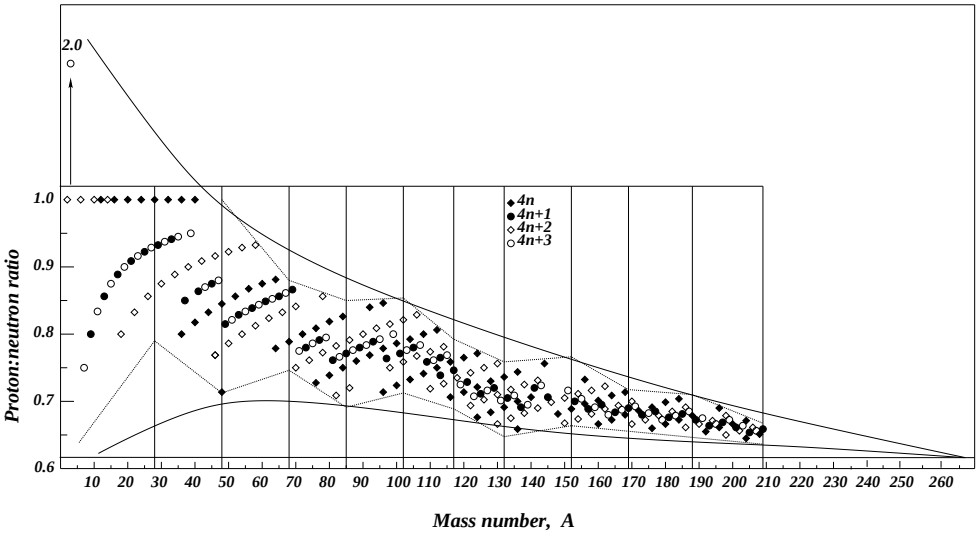

Fig. 5 *Using half-life as criterion the naturally occurring stable nuclides can be divided into four series of mass number A*(mod4)$\equiv 0,1,2,3$*, i.e two even series of 81 and two odd series of 51, considered as the product of* α*-particle addition [7]. A plot of the ratio* Z/N *vs A defines a converging field of stability, in line with the presumed periodicity of 24; condition (c).*

spiral. Noting that the numbers on each cycle add up to

$$\sigma(j+1) = \sum_{n=24j}^{24(j+1)} n = (2j+1)300\,,\; j = 0,1,2,\ldots$$

such that $\sigma_i = a, 3a, 5a, 7a \ldots \quad (a = 300)$, these odd-number coefficients were likened to the degeneracy of spherical electronic shells with spectroscopic notation s, p, d, f.

Re-interpretation of the sums as electron pairs over all stable nuclides, suggests

(a) A total[1] of 300 different nuclides;
(b) 100 different elements ;
(c) nuclide periodicity of 24;
(d) elemental periodicity of 8 .

[1] 300 isotopes of 100 elements, with $Z/N = 1$ are synthesized by α-particle addition in massive stellar objects. In interstellar space radioactive decay terminates at 264 stable isotopes of 81 elements.

This interpretation is supported [7] by analysis of the neutron imbalance of stable atomic species as a function of mass number, shown in Fig. 5. The region of nuclide stability is demarcated here by two zig-zag lines with deflection points at common values of mass number *A*. Vertical hem lines through the deflection points divide the field into 11 segments of 24 nuclides each, in line with condition (c). This theme is developed in more detail in the paper on Atomic Structure in this volume [8]. Defining neutron imbalance as either Z/N or $(N-Z)/Z$ the isotopes of each

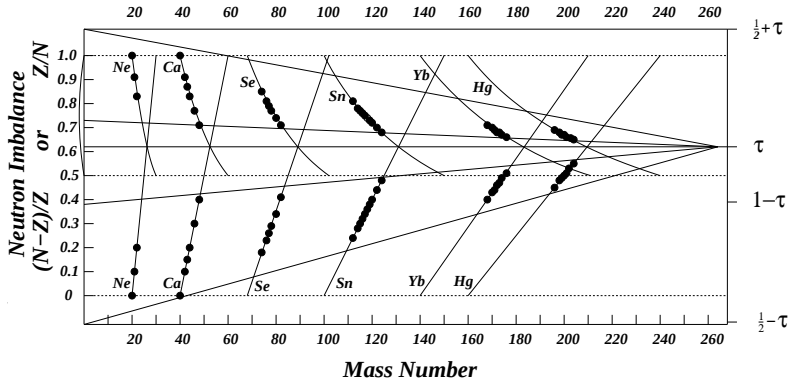

Fig. 6 *Neutron imbalance of atomic nuclei is defined either by the ratio Z/N or the relative excess $(N-Z)/Z$. As functions of mass number these quantities map the isotopes of a given element to respective circular segments and straight lines, the intersection of which defines the golden ratio.*

element, as shown in Fig. 6, map to either circular segments or straight lines that intersect where

$$\frac{Z}{N}=\frac{N-Z}{Z}\,,\ i.e.\quad Z^2+NZ-N^2=0,$$

with solutions of

$$Z=\tfrac{1}{2}N(1\pm\sqrt{5})\equiv\tau N.$$

This result provides the exact value of the convergence limit of Z/N first identified by William Harkins [9] as 0.62 according to the curves in Fig. 5.

To show that the periodic table of the elements is a subset of the more general nuclide periodicity, the data of Fig. 5 are replotted on axes of Z/N *vs* Z, as in Fig. 7.

In Fig. 7 the hem lines are no longer vertical, but still divide the field into 11 groups of 24. A remarkable feature of the diagram is the way in which the hem lines intersect the horizontal line $Z/N=\tau$ at points, which rounded off to the nearest integer, correspond with familiar values of atomic number that represent the closure of periodic subgroups:

$$10(2p),18(3p),28(3d),36(4p),38(5s),46(4d),48(5s),56(6s),62(4f:6/8),70(4f),80(5d)$$

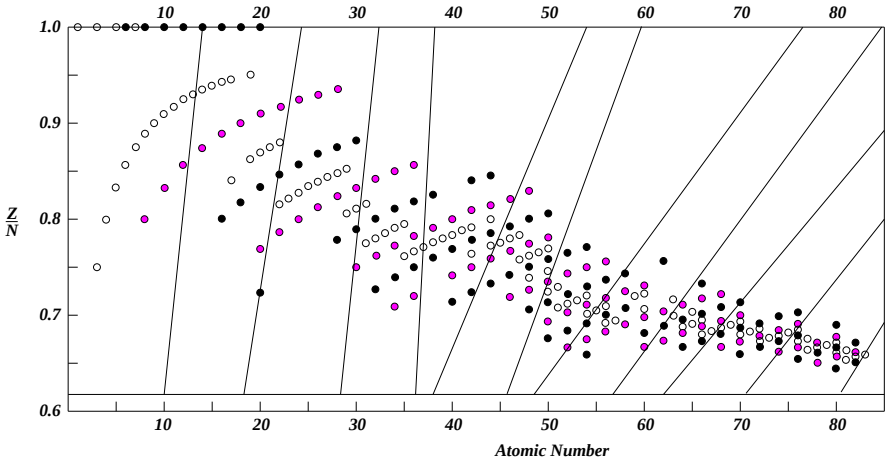

Fig. 7 *The periodic distribution of stable nuclides as a function of atomic number. Open circles represent odd mass numbers and the filled circles the two even mass-number series. The hem lines that define the nuclide periodicity of 24 are no longer parallel to the Z/N axis and their points of intersection with the lines at $Z/N = \tau$ and 1 are of special importance in the definition of elemental periodicity as a subset of the nuclide periodic function.*

Extrapolated to $Z/N = 1$ the points of intersection represent an inverted periodic table:

$$14(4f), 24(3d), 32(1s), 38(3p), 54(5f), 60(4p), 76(5p), 84(6p), 94(5d), 100(7p).$$

The only known mechanism that could cause such an inversion is a state of extremely high pressure [10]. We conjecture that the unit ratio of Z/N coupled with high pressure describes ideal conditions for the build-up of 300 nuclides[2] of 100 elements by $\alpha-$particle fusion in massive stellar objects, explaining conditions (a) and (b).

The cardinal points of intersection of the hem lines of Fig. 7 at $Z/N = 1.04$ are arranged symmetrically about $Z = 51$. On identification of the points $Z = 0$ and 102 a closed function is generated. Operating with the same element of mirror symmetry on the hemlines two sets, characteristic of both nuclides and anti-nuclides, are generated as shown in Fig. 8.

By following the hem lines from $Z/N = 0$ to 1.04 and back to zero, through the involution, a completely closed set is traced out, as shown in Fig. 9. Closed in four dimensions the resulting topology defines real projective space. Possible implications of this construction on molecular shape are discussed in the final paper of this volume [11].

Like objects in the solar system (next section) the periodic table of the elements can also be rationalized by elementary number theory. As the ratio Z/N always rep-

[2] On release into interstellar space radioactive decay results in the survival of only 264 stable nuclides as two sets of 81 with $A = 2n$ and two sets of 51 with odd A.

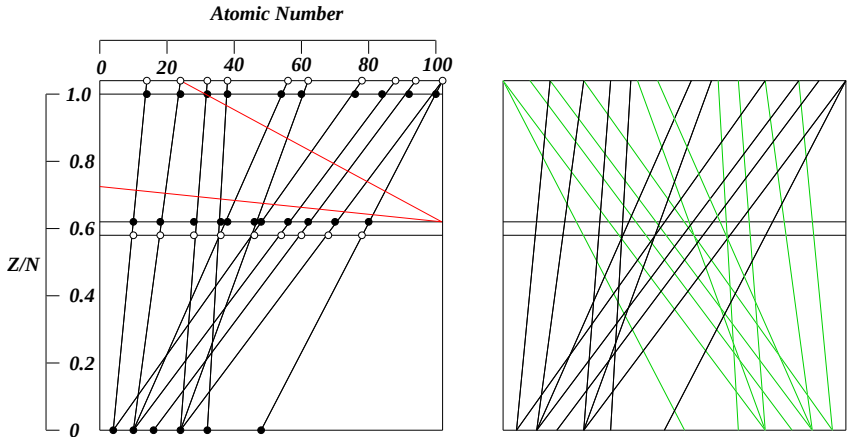

Fig. 8 *Variability of the periodic table of the elements depends on space-time curvature as shown in the frame on the left. The triangular segment defines the field of stability. The symmetrical version on the right is conveniently mapped to the surface of a Möbius band as in Fig. 9, but resolution is only possible in 4D projective space.*

resents a rational fraction, the pattern of Fig. 7 corresponds to some special ordering of rational fractions. The best-known order for the enumeration of rational fractions is known as a Farey sequence [12], which is generated by continued separate addition of numerators and denominators of adjacent fractions in the interval (0,1):

Fig. 9 *Schematic diagram to illustrate the involuted nature of the periodic relationship between matter and antimatter.*

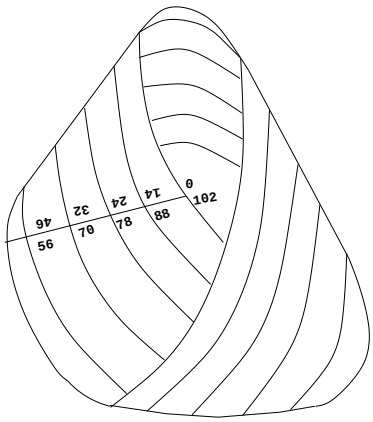

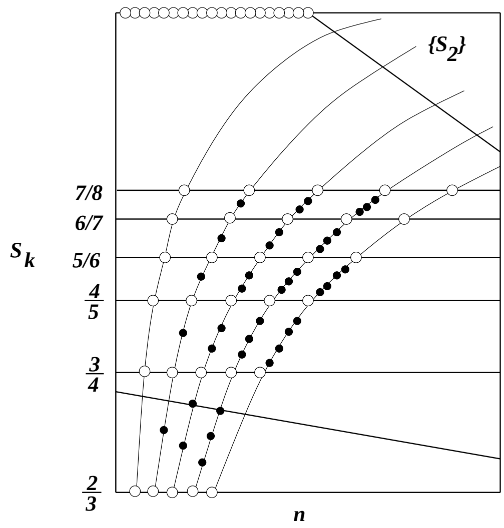

Fig. 10 *A plot of k-modular Farey sequences as a function of the natural numbers defines a set of infinite festoons that resembles the arrangement of nuclides in Fig. 5 and 7. The segment, obtained as a subset defined by limiting Fibbonacci fractions that converge from 1 to τ, and subject to the condition A(mod4)$= 0 \rightarrow 3$, corresponds to the observed field of nuclide stability.*

$$\begin{array}{ccccccccl}
\frac{0}{1} & & & & & & \frac{1}{1} & \mathscr{F}_1 \\
\frac{0}{1} & & & \frac{1}{2} & & & \frac{1}{1} & \mathscr{F}_2 \\
\frac{0}{1} & & \frac{1}{3} & \frac{1}{2} & \frac{2}{3} & & \frac{1}{1} & \mathscr{F}_3 \\
\frac{0}{1} & \frac{1}{4} & \frac{1}{3} & \frac{1}{2} & \frac{2}{3} & \frac{3}{4} & \frac{1}{1} & \mathscr{F}_4 \\
. & . & . & . & . & . & . & \mathscr{F}_n
\end{array}$$

The variation of Z/N with Z, shown in Fig. 7, mirrors the variation of the infinite k-modular sets of Farey sequences, defined by

$$S_k = \frac{n}{n+k} \quad , \quad (n,k) = 0,1,2,\ldots, \quad k = -\begin{vmatrix} h_i & h_{i+1} \\ k_i & k_{i+1} \end{vmatrix},$$

as a function of n. For simple Farey sequences $k = 1$. For example:

$$\begin{aligned}
\{S_0\} &= \frac{1}{1} \quad \frac{1}{1} \quad \frac{1}{1} \quad \frac{1}{1} \quad \ldots \text{modulus } 0 \\
\{S_1\} &= \frac{0}{1} \quad \frac{1}{2} \quad \frac{2}{3} \quad \frac{3}{4} \quad \frac{4}{5} \ldots \text{mod } 1 \\
\{S_5\} &= \frac{0}{5} \quad \frac{1}{6} \quad \frac{2}{7} \quad \frac{3}{8} \quad \frac{4}{9} \quad \frac{1}{2} \ldots \text{mod } 5
\end{aligned}$$

Part of these sets is plotted in Fig. 10 with the converging stability limits shown.

Each point within the triangle of stability represents a potential nuclide. However, naturally occurring nuclides are limited to four series of mass numbers $A(\text{mod}4) \equiv 0 \rightarrow 3$, interpreted to correspond to a process of nucleogenesis based on the fusion

of $\alpha-$particles to yield two even series of 81 members each and two odd series with 51 members [7]. Significantly, by this procedure all stable nuclides are identified correctly, except for a few $\alpha-$unstable ones. Isotopes of elements 43 and 61 are excluded naturally. For $n = Z$ isotopes of the same element are mapped to the same vertical line.

More simply, a plot of the unimodular Farey sequence

$$\mathscr{F}_4 = \left\{ \frac{0}{1}\,\frac{1}{4}\,\frac{1}{3}\,\frac{1}{2}\,\frac{2}{3}\,\frac{3}{4}\,\frac{1}{1} \right\}$$

as Ford circles [13], directly represents the periodic table as in Fig. 11.

As discussed in the paper on Atomic Structure [8] touching Ford circles have radii and y-coordinates of $1/2k_i^2$ and x-coordinates of h_i/k_i. The resulting map of $\mathscr{F}_4$ converts into the periodic table through the reciprocal radii of the numbered circles. Condition (d) is clearly implied.

It all seems to hang together. To account for such consilience, Plichta [6] conjectured that numbers have real existence in the same sense as space and time. A more conservative interpretation would link numbers, through the golden ratio, to the curvature of space-time. A common inference is that the appearance of numbers as a manifestation of the periodicity of atomic matter is due to a spherical wave structure of the atom. A decisive argument is that the full symmetry, implied by the golden ratio, incorporates both matter and antimatter as a closed periodic function with involution, as in Fig. 9, in line with projective space-time structure.

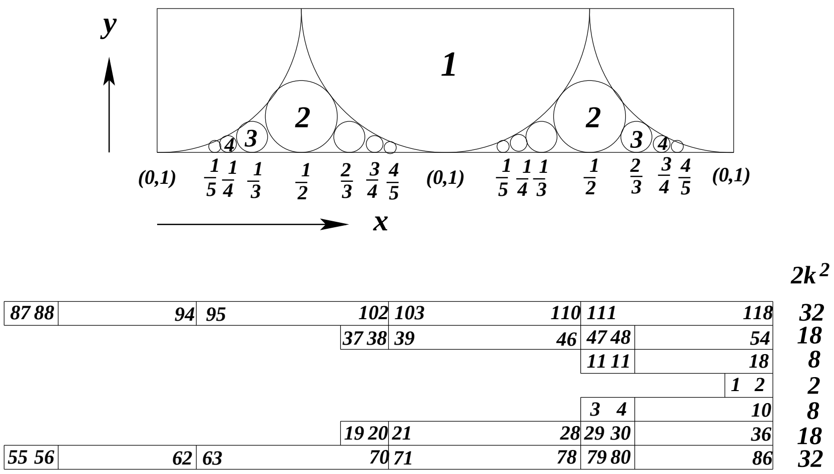

Fig. 11 *Mapping of the periodic table of the elements as the reciprocal radii of the $\mathscr{F}_4$ unimodular Ford circles.*

4 Commensurability in the Solar System

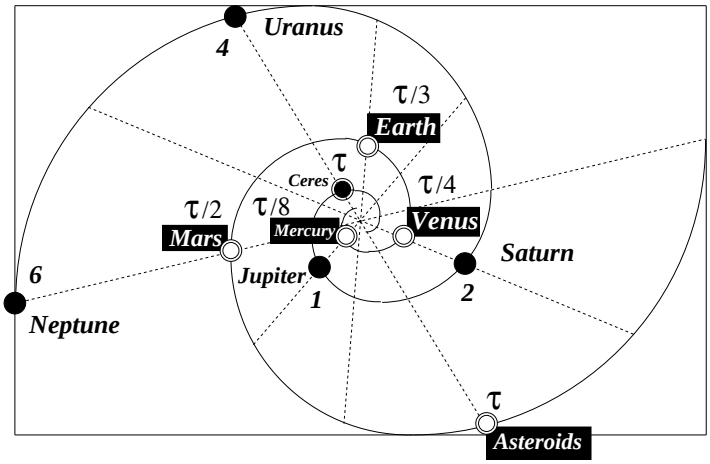

Fig. 12 *Simulation of planetary orbits by golden-spiral optimization. With the mean orbital radius of Jupiter as unit the outer planets are on orbits defined by integral multiples thereof. On the same scale the asteroid belt is at a distance τ from the sun and the inner planets have orbital radii of τ/n. For clarity the inner planets are shown on a larger self-similar scale.*

Like the golden ratio, golden spirals give a description of a diversity of natural phenomena such as the shape of nautilus shells, tropical hurricanes and spiral galaxies [1]. Golden spirals have the property of self-similarity, or invariance with respect to scale transformation, in which small parts of a structure have geometrical properties that resemble the whole structure or large parts thereof. Numerically, both golden ratio and golden spiral are described by the convergence of Fibonacci series. The convergence properties have been put to scientific use in the theoretical reconstruction of atomic periodicity [7] and the solution of optimization problems in engineering [14]. As a significant demonstration we show that the distribution of all matter in the solar system is correctly predicted by golden-spiral optimization. The assumption is that in a spiralling dust cloud matter accumulates at specific points along the spiral, specified by a *convergence angle*. The result for a convergence angle of $(180/5)^\circ$ is shown in Fig. 12.

The mean orbits of all planets, including Ceres, the largest asteroid, are correctly predicted [15] by the relative distances from the spiral centre. With the orbital radii expressed as rational fractions, a quantized distribution of major planets, as numbered, is revealed. On this scale the orbit of Ceres measures τ and those of the inner planets as rational fractions of the golden ratio. The same pattern was shown to repeat itself for the orbital motion of planetary moons and rings [15].

From this observation we infer self-similarity on a cosmic scale, from atoms to galaxies, which implies the same numerical basis for the atomic models of Nagaoka

[16] and Bohr, assumed self-similar with the rings of Saturn and the planets, respectively. In principle the periodic accumulation of extranuclear electron density on an atom could also be optimized by specifying an appropriate convergence angle.

5 Atomic Structure

The Ford circles that represent the Farey sequence of order 4 represents the periodic table of the elements in complete detail. In particular, they predict the appearance of electron shells with $n = 1,6$, consisting of 2, 8, 8, 18, 18, 32 electrons, in this order.

This arrangement is ideally suited to optimization by a golden spiral. A chemically meaningful solution results by stipulating a divergence angle of $4\pi/(2n-1)$, as explained in the paper on Atomic Structure [8]. The resulting distribution has extrema at integral distances of n^2 from the nucleus. If we assume that an electron cannot approach the nucleus more closely than the Bohr radius of a_0 the distribution can be considered as a spherical standing wave with zero surface at a radius a_0 and nodal surfaces at all n^2a_0. With the electron count known from the periodic function the mean electron density within each shell follows immediately. The predicted distribution scales directly to the Thomas-Fermi statistical model of the atom, and the periodicity for individual atoms agrees with the Hartree-Fock results, as shown in Fig. 13.

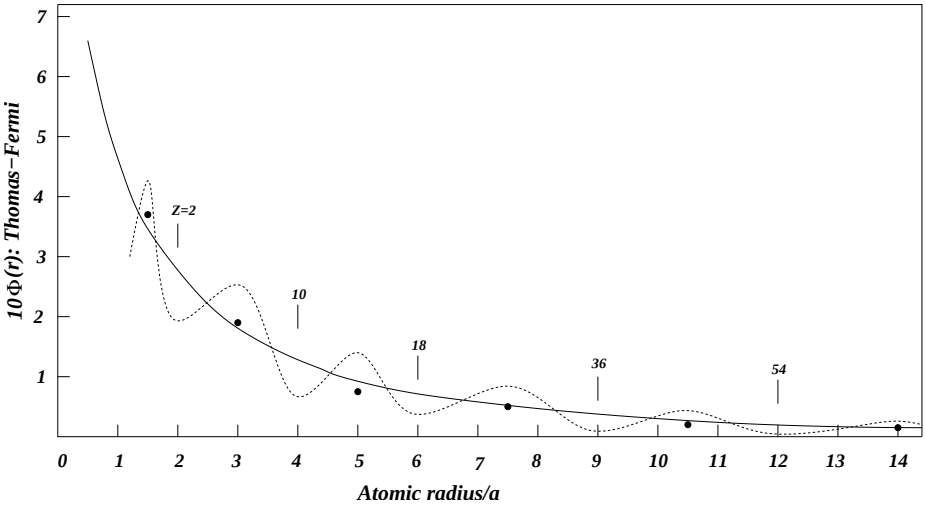

Fig. 13 *Simulation of Thomas-Fermi and Hartree-Fock electron densities for unit atoms as described later on [8]. The calculated points are those predicted by golden-spiral optimization and scaled to match the Thomas-Fermi curve, shown as a solid line. The dotted curve simulates the HF result.*

6 Electronegativity

The ground-state electron configuration of an atom is of limited value as a predictor of chemical affinity since most chemical reactions result from interaction between atoms in an activated valence state. The valence state is commonly considered to be reached by thermal activation, which gives rise to high-energy atomic collisions. Activation by uniform compression of an atom, which is not a feasible laboratory procedure, is more convenient for mathematical simulation [10, 17]. Computerized compression is done by Hartree-Fock simulation with modified boundary conditions that restrict wave functions to a finite sphere [17]. All electronic energies move to higher levels as the limiting radius is reduced, until a single electron reaches the ionization limit. At this point the valence electron, decoupled from interaction with the nucleus, is confined to a sphere of characteristic radius r_0, interpreted as the *ionization radius*. This is a standard problem in free-electron quantum theory which calculates the energy of an electron, which is uniformly spread across the confining sphere, as [18]:

$$E_g = \frac{h^2}{8mr_0^2}.$$

When the valence electron reaches the ionization limit its potential energy with respect to the nucleus goes to zero and in uniform distribution it has no kinetic energy. The calculated confinement energy (E_g) can therefore only represent quantum potential energy, defined as [19]:

$$V_q = -\frac{\hbar\nabla^2 R}{2mR}.$$

This equation is solved by E_g, on the basis of which the valence electron is now interpreted to have reached an activated state at a chemical potential of E_g. This state defines *electronegativity*. To be in line with traditional practice it is formally defined as $\chi = \sqrt{E_g}$, with r_0 in Å units and E_g in eV [20].

Starting from the numerically optimized valence density in a ground-state valence shell the radius of an equivalent sphere, which accommodates this total density at a uniform level, is readily calculated by simple geometry. There is very good correspondence with Hartree-Fock values of ionization radii, with the added advantage of higher accuracy for the chemically important second period elements where the HF results are notoriously unreliable [17, 21].

By the use of elementary number theory, to simulate uniform distribution of a valence electron over the ionization sphere, a complete set of ionization radii and electronegativities is now available for the simulation of a whole range of chemical properties as described in the papers to follow.

7 Bond Order

On looking for a relationship between ionization radius and the chemistry of homonuclear covalent interaction the classification into single and multiple bonds[3] is followed as a first approximation. An immediate observation, valid for most single bonds is a constant value of the dimensionless distance

$$d' = d/r_0 = 0.869,$$

where d is the experimentally known covalent interatomic distance. Notable exceptions occur for F–F, O–O and I–I with $d' = 0.935$. A similar trend is observed for most double and triple bonds. For the smaller number of quadruple dimetal bonds $d' = \tau$, to good approximation. Assuming zero-order interaction to occur at $d = r_0$, it follows that d' converges from unity to τ with increasing bond order, corresponding to a divergence angle of $\pi/2$ on a golden spiral.

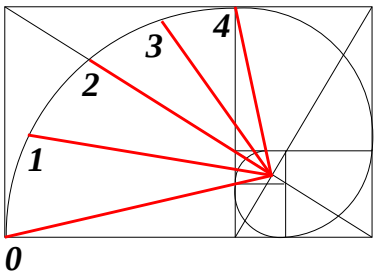

Fig. 14 *Simulation of integer bond orders on a golden spiral. The dimensionless distances $d' = 1$ and τ, which represent zero and fourth order respectively, must, by definition, be separated by a convergence angle of 90° on a golden spiral. Convergence angles for intermediate integer and half-integer orders follow directly.*

Divergence angles of $\pi/8$ and $\pi/16$ for integer and half-integer bond orders are implied and shown in Fig. 14. This solution corresponds with the empirical values derived before, *i.e.*:

b	0	$\frac{1}{2}$	1	$1\frac{1}{2}$	2	$2\frac{1}{2}$	3	$3\frac{1}{2}$	4
d'	1.0	.935	.869	.804	.764	.724	.683	.658	.618

The corresponding numerical solution defines bond order, b, by the equation

$$d' = j_b \tau^n$$

where both n and the covariant integer coefficient j_b, for bond order b, depend in a simple way on Fibonacci numbers. This procedure is described more fully in the Covalence paper [25].

The quantized variation of bond order may be rationalized by viewing overlapping charge spheres as spherical standing waves. These waves interfere construc-

[3] Bond order, assumed to stipulate the number of electron pairs in covalent interaction, although a poor measure of bond strength [22, 23, 24], is a convenient general working model.

tively at specific interatomic distances that depend on wavelength. Destructive interference that occurs at intermediate distances tend to destabilize the interaction and to prevent continuous variation of bond order. Distortion of the interference pattern requires work, as measured by bond-stretching force constants.

8 Covalent Interaction

With the relationship between ionization radius and bond order in hand, the calculation of covalent interaction parameters becomes an almost trivial exercise. The common volume, ε, between overlapping spheres of radius r_0 at characteristic separations d' for given bond order, and considered proportional to dissociation energy, varies in a quantized fashion similar to d'. This allows definition of a dimensionless dissociation energy $D' = Dr_0/K$, as explained in the paper on Covalent Interaction [25]. K is a dimensional constant. Noting the connection of ε with spherical volume one looks for a dependence of the type

$$\frac{D_x r_0}{K} = D' \propto r_0^3.$$

First-order homonuclear interactions are seen to obey the rule, $D_x = Kr_0^2\tau^n$, where n correlates positively with bond order.

By taking electronegativity difference into account dissociation energy for heteronuclear interactions are calculated as

$$D_c = Kr_0^3(1)/r_0(2) \quad ; \quad r_0(1) > r_0(2).$$

Exhaustive testing has shown the formula to hold for all heteronuclear interactions of any order.

Resistance against change of bond order is measured as a harmonic stretching force constant. It depends on the relative energies of adjacent bond orders and on the slope of the linear curve that describes continuous change of bond order. In general

$$\tfrac{1}{2}k_r = \frac{\Delta D'}{(\Delta d')^2}\,.$$

Estimation of $\Delta D'$ is facilitated by the special property of the golden ratio: $\tau^n - \tau^{n+1} = \tau^{n+2} = \tau^+$, in shorthand notation. In the common units of Ncm^{-1} the general expression becomes

$$k_r = \frac{4.615\tau^+ s}{(\Delta d')^2 r_0(1)\cdot r_0(2)}.$$

The formula can be demonstrated convincingly, applied to well-researched series of diatomic molecules. Individual bonds in larger molecules are less well described, but MM force constants derived by this method are in good agreement with other general parameters [26].

Exploiting the possibility of representing polarization effects in diatomic molecules many dipole moments, especially for diatomics such as the alkali halides can be simulated with a high degree of confidence. A general lack of experimental values to serve as empirical guidance has so far prevented the development of the method to its full capacity.

9 The Physical Meaning

Based on elementary number theory we have arrived at a computational scheme that works unexpectedly well for the simulation of chemical phenomena. The problem is to find a plausible interpretation to connect the abstract model with the concrete. The statistical scheme of probability densities and point particles adopted in physics does not provide a satisfactory answer in this case. We are forced to enquire more deeply into the fundamental nature of matter.

The only fundamental theory that considers the genesis of matter is the theory of general relativity. It is formulated in 4D space-time as a set of field equations,

$$G_{\mu,\nu} = kT_{\mu,\nu} \quad , \quad \mu,\nu = 0,3$$

that balances space-time curvature against the matter-energy content of the system. The implication of this relationship is that the appearance of matter is unequivocally linked to the curvature of space-time. In particular, matter cannot exist in Euclidean space [27].

For convenience humans consider their living space to be Euclidean and even advanced cosmologies are still formulated in such terms. In order to operate in Euclidean space it is necessary to separate the mathematically equivalent variables of Einstein's equation into a universal time variable and the three familiar variables of coordinate space. This operation destroys the 4D field equations and no longer provides any insight into the nature of matter. For this reason the existence of matter is added to physical theory as an *ad hoc* postulate — the prescription of classical Newtonian mechanics.

Quantum mechanics follows the same prescription, by separating the 4D potential function, formulated as

$$\Box^2 \Phi = 0 \quad \text{into the wave equation} \quad \left(\nabla^2 - \frac{1}{c^2}\frac{\partial^2}{\partial t^2}\right)\Phi = 0.$$

The suspicion that this separation of variables, although mathematically sound, leads to a less than perfect description of quantum systems is confirmed [28] by statistical testing of the seminal equation that relates the frequency of the energy radiated or absorbed by a H atom to the integers in the Rydberg formula

$$\bar{\nu} = R\left(\frac{1}{n^2} - \frac{1}{k^2}\right).$$

This is the equation of a straight line, which, for the Lyman series with $n = 1$, reduces to

$$\bar{\nu} = -R/k^2 + R$$
$$(y = mx + c)$$

A plot of $\bar{\nu}$ *vs* $-1/k^2$ should be linear, with equal slope and intercept. The most reliable and accurate data available fail this test statistically [28]. The discrepancy is not large but significant and reminiscent of the spectroscopic red shift measured in galactic light. The common origin of these discrepancies cannot be a Doppler effect and is probably due to space-time curvature.

In the 4D equation space and time coordinates are inextricably entangled. Its mathematical solutions are hypercomplex functions, or quaternions, without a commutative algebra. Quaternions are used to describe what is known as spherical rotation, also called the spin function, and the complex rotation known as the Lorentz transformation of special relativity.

The separated 3D wave equation can no longer describe any of these fundamental rotations. For this reason, the discovery of electron spin necessitated its introduction into quantum theory as another *ad hoc* postulate. The anomalous consequence is the unphysical situation of a point particle with spin. Only part of the spin function survives solution of the 3D wave equation, in the form of a complex variable interpreted as orbital angular momentum. In the so-called p_z-state it has the peculiar property of non-zero orbital angular momentum with zero component in the direction of an applied magnetic field. This is the price to pay for elimination of spherical rotation.

Despite this anomaly the complex angular-momentum function can be used to rationalize many features of stereochemistry. It represents the only vector quantity in wave mechanics which could interact with an applied magnetic field. It accounts for the so-called *Faraday effect*, which is a property of achiral molecules in an applied magnetic field to rotate the plane of polarized light. It is easy to demonstrate that atomic orbital angular momentum vectors always line up anti-parallel in diatomic interaction and continue to do so in more complicated symmetrical atomic assemblies on molecule formation. It is only in chiral molecules, without reflection or inversion symmetry, that total quenching of orbital angular momentum is no longer possible. The residual orbital angular momentum with its associated magnetic moment is responsible for optical activity in such cases.

This tendency to quench orbital angular momentum may be used to good effect to predict the mutual orientation of sub-molecular fragments (radicals) on forming a molecule. The symmetry of substituted methanes and other small molecules has been successfully analyzed by this method [29, 18]. Where quenching requires a specific mutual orientation in 3D the interaction exhibits steric rigidity. By systematic use of these principles it is possible to predict the 3D structure of complex molecules, without allowing for the effects of non-bonded and torsional interactions. The resulting structures are suitable as trial input for optimization by MM [26].

These positive results are not without exception. Immediately obvious is the anomalous optical effects observed in a homochiral series such as the biologically

active amino acids. Despite their uniform chirality[4] only about half of them rotate an optical plane of polarization in the same sense. The orbital angular momentum of 3D wave mechanics is clearly inadequate as an explanation of optical activity in such detail. For a deeper understanding of the phenomenon it is necessary to reconsider the effect of 4D molecular symmetry.

The discovery of quantum mechanics was seen as a dramatic departure from classical theory because of the unforeseen appearance of complex functions and dynamic variables that do not commute. These effects gave rise to the lore of quantum theory as an outlandish mystery that defies comprehension. In our view this is a valid assessment only in so far as human beings have become evolutionary conditioned to interpret the world as strictly three dimensional. The discovery of a 4D world in special relativity has not been properly digested as yet, because all macroscopic structures are three dimensional. Or, more likely, minor discrepancies between 4D reality and its 3D projection are simply ignored. In the atomic and molecular domains, where events depend more directly on 4D potential balance, projection into 3D creates a misleading image of reality. We argue this point on the basis of different perceptions of chirality in 3D and 2D respectively. As shown in Fig. 15 inversion

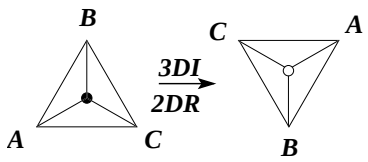

Fig. 15 *Diagram to show that three-dimensional inversion (3DI) could be mistaken as rotation (2DR) in two dimensions.*

of a chiral tetrahedron, with the base ABC in a fixed 2D plane, changes the 3D chirality, but appears as a simple rotation in 2D. We anticipate similar discrepancies between 4D symmetry and its projection into 3D as responsible for the irregular variation of optical activity as a function of 3D chirality.

The appearance of non-commuting quantum variables can now also be traced back to the non-commutative algebra of 4D hypercomplex functions. On projection into 3D by the separation of space and time variables the quaternion variables are reduced to complex functions that characterize orbital angular momentum, but the commutation properties remain. Not appreciating the essence of complex wave functions, an unfortunate tradition to reduce them to real functions, has developed in quantum chemistry. These real orbitals and basis sets only have classical meaning. Relations in the complex plane, which describe orbital angular momentum, are reduced to harmonic oscillations on a real line.

Topologists describe the projection from four to three dimensions in terms of an underlying 4D curved space-time and a Euclidean space, tangent to the 4D manifold, with a universal time coordinate. The only 4D sphere with a continuous group structure is $\mathbb{S}^3$ and the space of antipodal points on $\mathbb{S}^3$ is known as *projective space*, and denoted by $P_3(\mathbb{R})$ [32]. A section through projective space is a Möbius band —

[4] For the sake of simplicity we do not consider degrees of chirality as distinguished by chirality functions [30, 31]

a 2D construct which cannot be embedded in 2D space. Correspondingly a Möbius band, closed on all sides, cannot be embedded in 3D space. Projective space, although hard to visualize is the physically most likely structure of the underlying 4D curved space-time.

The previous statement is based on the results of reformulating the theory of general relativity in projective space, as a model of unified electromagnetic and gravitational fields [33]. On transformation of the electromagnetic part into tangent space the relationship between 3D and 4D potentials is of the form [34]:

$$\left(\frac{e}{mc^2}\right) V_j = \frac{\sqrt{5}}{2}\varphi_j = (\tau + \tfrac{1}{2})\varphi_j \,.$$

Here is the first inkling about the universal importance of the golden ratio. If it measures the relationship between underlying space and tangent space it is not surprising for it to show up in the apparent structure of so many objects from atoms to galaxies. It might even be interpreted as a measure of space-time curvature.

The relationship between space-time curvature and the golden ratio amounts to little more than a suspicion, based on the factor that converts the electromagnetic field from projective space into an affine theory. To account for the ubiquitous appearance of golden spirals in self-similar chemical and cosmic structures we may look for a related factor in the construction of a golden spiral from the series of gnomonic circular segments as in Fig. 3. The ratio between arc length, $\pi r/2$, and chord, $\sqrt{2}r$, *i.e.* between curve and tangent, $\pi/(2\sqrt{2}) = 1.111 \simeq \sqrt{5}/2$, supports the suspicion. If the curvature of space-time depends on the golden ratio it is no longer surprising to find that structures of all sizes are self-similar and conditioned by τ. To summarize: the golden ratio features in the packing of nucleons [7], the electronic structure of atoms, the details of chemical interaction, the periodicity of atomic matter [2], the structure of nanoparticles [3], botanical phyllotaxis, planetary and solar systems [15], spiral galaxies and the large-scale structure of the universe [27].

It is reasonable to expect that any growing structure should follow this curvature and for 3D observers to find the imprint of the golden ratio everywhere, also in the structure of molecules. It would not be surprising to find the golden ratio among the topological features of macromolecules or even reflected in the torsion angles within smaller molecules [35].

We are reaching the conclusion that the modelling of molecular structure by number-theoretic golden parameters may well be a fundamentally appropriate procedure. At this stage, the simulation of important internal molecular structural parameters, with the exception of torsion angles, can be undertaken with confidence. It is quite clear however, that at the present very early stage of development, the optimized structures, for many reasons, are quite crude, and the optimization of the functional forms and parameter sets, based on experimental data, may be required. The final objective might be structure optimization by MM, using a generic force field based on number theory.

10 Molecular Mechanics

Molecular modelling by minimization of the steric energy starts from an assumed structure in which the rigid bonds are replaced by flexible springs of characteristic lengths and strengths (force constants in Hookes law); similar harmonic potentials are used to model angular distortions and torsional flexibility [36].

In the fully empirical approach a characteristic bond length and a matching force constant are assigned to a molecular fragment to reproduce an observed interatomic distance on energy minimization. In the number theory approach [26] an ideal bond length, free of strain, is calculated as a function of ionization radii and bond order. For smaller, chemically important atoms, it may be necessary to allow for the distortion of atomic sphericity by first-neighbours. Calculation of the stretching force constant requires, in addition, an estimate of the diatomic dissociation energies at different bond orders, which are obtained as functions of ionization radii and the golden ratio. That is, modeling of bond distances is based on generic parameters, and these may be computed very efficiently for all possible combinations of the entire periodic table, various oxidation and electronic ground states included.

Second-neighbour interactions are optimized empirically from a characteristic valence angle and a matching angle-bending force constant. In the number theory approach 1,3-interactions are calculated as a lower-order interaction with an associated stretching force constant, readily converted into an angle-bending force constant, as needed. The interactions between more distant neighbours are considered as weak bonds with a minimum at the characteristic van der Waals separation. In number theory these are zero-order interactions. The parameters generated by number theory would therefore be ideally suited for use with a Central Force Field [37] in which two-body forces between atoms are used exclusively, in place of bond angles and torsion angles.

Torsional interactions are empirically modelled with a periodic function based on local geometry around the central bond. This problem has not yet been studied in number theory. Neither have any of the other parameters such as cross-term interactions, electrostatic interactions, out-of-plane deformation, and more specific electronic interactions been considered for number-theory-based simulation [38, 39, 40, 41].

The purpose of the number-theory analysis is not primarily to produce another force field (to which all these special features might be added), but rather to demonstrate that the MM approach is fundamentally sound, and to provide a simple approach for efficiently computing generic force field parameters which might be used directly or after optimization based on experimental data. Other generic force field approaches have been used in various universal force field methods [42, 43, 44]. Important additional contributions that number theory can make to MM simulations are to also provide generic force field parameters for interactions that involve metal ions, and possibly also to efficiently compute charge distributions based on electronegativities [26, 45].

11 Chemical Matter

As in wave mechanics, the simulation of chemical phenomena by number theory is characterized by the appearance of integers; in this case associated with chemical structures and transformations. An obvious conclusion is that the elementary units of matter should be viewed as wave structures rather than point particles, which is consistent with the first appearance of matter in curved space-time. Even 3D wave packets behave in a manner convincingly like ponderable matter and rationalize the equivalence of mass and energy in a natural way. There is no compelling reason why this simple model should be obfuscated with the notion of wave/particle duality. And more so on realising that the wave-like space-time distortions are strictly 4D structures. In response to environmental pressure an electronic wave packet can shrink to the effective size of an elementary particle or increase to enfold a proton as a spherical standing wave.

A wave structure of the electron, which is routinely verified by electron diffraction, facilitates the understanding of atomic structure and concepts like bond order. It provides a logical explanation of the photoelectric effect as an interaction between waves, doing away with photons and wavicles at the same time.

Interacting elementary wave packets are expected to coalesce into larger wave packets. All extranuclear electrons on an atom therefore together constitute a single spherical standing wave with internal structure, commensurate with a logarithmic optimization pattern. In the activated valence state the central core of the wave packet is compressed into a miniscule sphere, compared to the valence shell which dominates the extranuclear space up to the ionization radius.

When atoms interact, these standing waves interfere to generate an interference pattern that determines the molecular charge distribution. Closer interaction happens stepwise in stages, described in chemical terminology as increasing bond order. Charge densities recorded in X-ray crystallographic studies, clearly resemble such a distribution.

Acknowledgements Financial support by the Alexander von Humboldt Foundation is gratefully acknowledged. We acknowledge the input of Casper Schutte during many informative discussions.

References

1. Livio M (2002) The Golden Ratio. Review, London.
2. Boeyens JCA (2003) J Radioanal Nucl Chem 259:33.
3. Li C, Zhang X, Cao Z (2005) Science 309:909.
4. Coxeter HSM (1989) Introduction to Geometry. 2nd ed. Wiley, NY.
5. de Chancourtois AEB (1889) Nature 41:186.
6. Plichta P (1998) God's Secret Formula. Element Books, Boston.
7. Boeyens JCA, Levendis DC (2008) Number Theory and the Periodicity of Matter. Springer.com.
8. Boeyens JCA (2012) Calculation of Atomic Structure. This volume.
9. Harkins WD (1931) Phys Rev 38:1270.
10. Goldman S, Joslin, C (1992) J Phys Chem 96:6021.
11. Boeyens JCA, Levendis DC (2012) All is Number. This volume.
12. Hardy GH, Wright EM (1979) An Introduction to the Theory of Numbers. 5th ed. University Press, Oxford.
13. Ford LR Sr (1938) Amer Math Monthly 45:586.
14. Boltyanskii VG (1971) Mathematical Methods of Optical Control. Translated from the Russian by Trirogoff KN and Tarnove I.
    Holt, Reinhart and Winston, New York.
15. Boeyens JCA (2009) Physics Essays 22:493.
16. Nagaoka H (1904) Phil Mag J Sci 7:445.
17. Boeyens JCA (1994) J Chem Soc Faraday Trans 90:3377.
18. Boeyens JCA (2008) Chemistry from First Principles. Springer.com
19. Bohm D (1952) Phys Rev 85:166.
20. Boeyens JCA (2008) Z Naturforsch 63b:199.
21. Herman F, Skillman S (1963) Atomic Structure Calculations. Prentice-Hall, NJ.
22. Boeyens JCA (1982) J Crystall Spectr Res 12:245.
23. Kutzelnigg W (1973) Angew Chem 85:551.
24. Pauling L (1960) The Nature of the Chemical Bond. Cornell University Press, Ithaca.
25. Boeyens JCA (2012) Covalent Interaction. This volume.
26. Comba P, Boeyens JCA (2012), Molecular shape, This volume.
27. Boeyens JCA (2010) Chemical Cosmology. Springer.com.
28. Schutte CJH (2012), This volume.
29. Boeyens JCA (2003) New Theories for Chemistry. Elsevier, Amsterdam.
30. Derflinger G (1991) in [46].
31. Ruch E (1972) Acc Chem Res 5:49.
32. Stillwell J (1992) Geometry of Surfaces. Springer-Verlag, Heidelberg.
33. Veblen O (1933) Projektive Relativitätstheorie. Springer-Verlag, Berlin. English translation in [27].
34. Veblen O, Hoffman B (1930) Phys Rev 36:810.
35. Boeyens JCA (2010) Int J Mol Sci 11:4267.
36. Comba P, Hambley TW, Martin B (2009) Molecular Modeling of Inorganic Compounds. 3rd Completely Revised and Enlarged Edition. Wiley-VCH, Weinheim.
37. Saunders M, Jarret RM (1986) J Comp Chem 7:578.
38. Comba P, Zimmer M (1994) Inorg Chem 33:5368.
39. Comba P, Hambley TW, Strhle M (1995) Helv Chim Acta 78:2042.
40. Root DM, Landis CR, Cleveland T (1993) J Am Chem Soc 115:4201.
41. Deeth RJ (2004) Struct Bonding 113:37.
42. Mayo SL, Olafson BD, Goddard III WA (1990) J Phys Chem 94:8897.
43. Rappe AK, Casewit CJ, Colwell KS, Goddard III WA, Skiff WM (1992) J Am Chem Soc 114:10024.
44. Shi S, Yan L, Yang Y, Fischer-Shaulsky J, Tatcher T (2003) J Comput Chem 24:1059.
45. Rappe AK, Goddard III WA (1991) J Phys Chem 95:3358.
46. Janoschek R (ed.) (1991) Chirality - From Weak Bosons to the $\alpha-$Helix. Springer-Verlag, Heidelberg.